Research Article

Modelling and Comparative Performance Analysis of a Time-Reversed UWB System

K. Popovski, B. J. Wysocki, and T. A. Wysocki

School of Electrical, Computer and Telecommunications Engineering, University of Wollongong, Northfields Avenue, Wollongong 2522, NSW, Australia

The effects of multipath propagation lead to a significant decrease in system performance in most of the proposed ultra-wideband communication systems. A time-reversed system utilises the multipath channel impulse response to decrease receiver complexity, through a prefiltering at the transmitter. This paper discusses the modelling and comparative performance of a UWB system utilising time-reversed communications. System equations are presented, together with a semianalytical formulation on the level of intersymbol interference and multiuser interference. The standardised IEEE 802.15.3a channel model is applied, and the estimated error performance is compared through simulation with the performance of both time-hopped time-reversed and RAKE-based UWB systems.

1. INTRODUCTION

Following the release for commercial applications in early 2002 [1], ultra-wideband (UWB) communications, or impulse radio, has seen significant attention. It is characterised by having a fractional bandwidth of more than 20%, or bandwidth occupancy greater than 500 MHz [2]. Due to the increased bandwidth, UWB is expected to support higher data rates than conventional narrowband systems. The two main competitors for the UWB standard are the "UWB Forum" direct sequence-based system, and the "WiMedia Alliance" orthogonal frequency division multiplexing based scheme [3]. Unfortunately, the IEEE body responsible for the UWB 802.15.3a standard has been disbanded, leaving the decision to be made by market forces [4].

A UWB scheme which has not seen as much attention is time hopped UWB (TH-UWB), which is similar in implementation to direct sequence UWB. In this system, pulses transmitted are either delayed in time (pulse position modulation (PPM)) or changed in amplitude (pulse amplitude modulation (PAM)) for data encoding. Users are multiplexed through code division multiple access based upon a family of orthogonal time hopping codes.

This paper deals with a TH-UWB system, utilising a "time-reversed" (TR) approach, which has its origins in un-

derwater acoustics [5]. This scheme has also been referred to as "prerake" [6]. While a conventional system would operate with the transmission of subnanosecond width Gaussian waveforms, a TR-UWB system uses the channel impulse response from the transmitter to the receiver as a transmit prefilter. The transmitted time-reversed signal retraces its path through the channel, resulting in an autocorrelation of the response being received [7–9]. This extends from work in underwater experimentation with soundwaves, as in [10]. These showed that when energy losses are small, wave equations guarantee that for each sound burst that diverges from a point, there exists a set of waves which would converge through the paths back to the point source.

Conventional UWB schemes such as TH-UWB have several commercially appealing aspects, including low implementation cost, and low power consumption [8]. Another benefit is that multipath components are capable of being fully resolvable, provided that the duration of each pulse is shorter than the difference between propagation delays of different multipath components [11]. Unfortunately, typical UWB indoor channel responses have a delay spread of approximately 80 to 200 nanoseconds, with 60 to 200 paths [12]. Some systems employ a time spacing between user transmissions that is close to or greater than the channel

response length. This is to ensure that the multipath dispersion has sufficiently passed.

TR-UWB, however, shifts the design complexity from the receiver to the transmitter. With the estimation of the channel impulse response, the transmitter is able to make the propagation channel perform the signal correlation. The received signal is focused in both time (temporal focusing) and space (spatial focusing) at the intended receiver, concentrating the sent energy with a spatial resolution of the order of the wavelength [7–9, 13–15]. Through temporal focusing, a TR-UWB system is capable of effectively mitigating intersymbol interference (ISI). Focusing also allows time-reversed communications to be more robust in the presence of narrowband interference relative to receiver-equalisation-based UWB [16].

Ultimately, there are fundamental drawbacks of a time-reversed system. These include

(i) determining the channel impulse response from the transmitter to the receiver for use in the former;

(ii) the possibility of channel correlation between users; and

(iii) the large time interval required to obtain the response in heterogeneous systems.

This paper discusses the modelling and comparative performance of a TR-UWB system. It is organised as follows Section 2 provides an overview into UWB and TR-UWB communications, Section 3 covers various signal degradations and error performance analysis, Section 4 overviews a UWB and TR-UWB simulation, together with a comparative analysis of the theoretical and simulated results for a time-reversed system. Finally, Section 5 gives all concluding statements and remarks.

2. SYSTEM EQUATIONS

2.1. Equalisation methods

While the concept of channel equalisation does present benefits in terms of user error performance, it inevitably leads to an increase in the level of complexity of the system. Increased memory, channel tracking, and additional processing are a few of the requirements, with the possibility of being incorporated into either the transmitter or the receiver.

Receiver side equalisation, which is more common in wireless communications, entails the collection of channel distorted energy, with increased receiver complexity. A RAKE structure is common in UWB communications in order to offset channel effects, with a branch dedicated to each arriving path encompassed in the decision process [17].

A common application of receiver equalisation is in sensor networks, where a collection of nodes each with one or more environment sensors, communicate to higher level node receivers which perform channel equalisation. This allows the sensor nodes to be simpler in design, also saving on energy. Existing sensor network methods include "BTnodes" [18] and Intel's "Imote" [19], both high bandwidth methods based upon bluetooth technology.
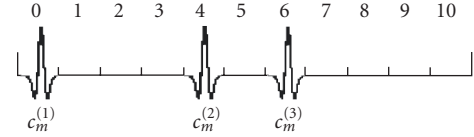

FIGURE 1: Positioning of pulses by a time-hopping code.

A disadvantage in receiver side equalisation is that RAKE receivers, for instance, grow linearly in complexity with an increase in the number of branches [13]. It has been proven that in order to collect about half of the energy in a transmission, RAKE receivers with more than 10 taps are required [20].

Transmitter side equalisation comprises of a shift in the design complexity to the transmitter side. An ideal application would be in actuator networks, where remote nodes are desired to be simple, inexpensive, and consuming minimal power.

Alternate equalisation measures include a time-reversed UWB adaptation whereby an MMSE equaliser is adopted at the receiver to increase energy collection [21]; and a receiver-side equalisation scheme encompassing MMSE decision feedback and the application of stochastic gradient descent algorithms [22].

2.2. Receiver-side equalisation

The signal $s^{(u)}(t)$ transmitted for the uth user in a time-hopped UWB system adopting a RAKE receiver, with equiprobable data $b_m^{(u)} \in \{-1, 1\}$ mapped through binary PPM with the time shift ε, is given by [23]

$$s^{(u)}(t) = \sqrt{E_{TX}(u)} \sum_{m=0}^{N-1} w\big(t - mT_f - c_m^{(u)} T_c - \varepsilon b_m^{(u)}\big), \qquad (1)$$

where $E_{TX}(u)$ is the uth user's signal energy, $w(t)$ is the base transmitted waveform of width T_m seconds, m is the frame number, and N represents the number of symbols within a single block of data. T_f is a single frame length, which is segmented into equally spaced intervals called "chips" of duration T_c. Finally, $c_m^{(u)}$ denotes the position within the particular frame (the chip number) that is occupied by the uth user's signal in accordance with a time-hopping sequence. If two users simultaneously occupy the same chip, a collision or "hit" occurs. The characterising parameters of these codes are the cardinality (N_h), which specifies the alphabet size; and the periodicity (N_p), which indicates the length of the code before it is repeated. This time multiplexing is shown in Figure 1, with $c_m^{(u)} \in \mathfrak{R}$, $0 \leq c_m^{(u)} \leq N_h - 1$. In the example, $c_m^{(1)} = 0$, $c_m^{(2)} = 4$, $c_m^{(3)} = 6$, and a frame of $N_h = 11$ chips is used.

With the data shift ε, and the pulse duration T_m, the remaining frame duration is defined as the "guard time" T_g, where

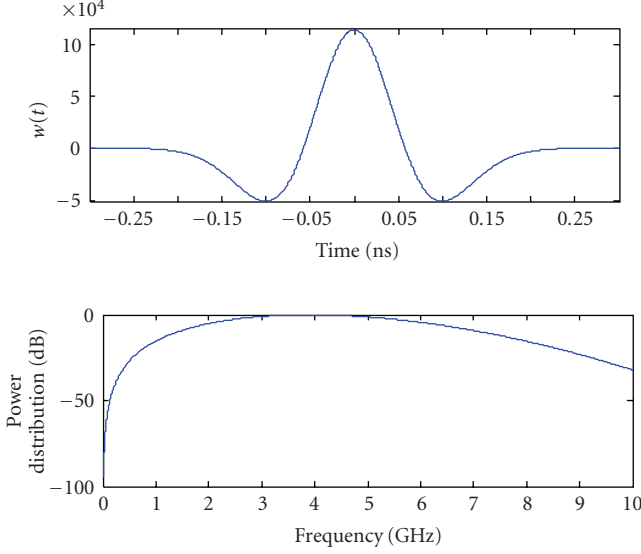$$T_g = T_c - (\varepsilon + T_m). \qquad (2)$$

FIGURE 2: Time and frequency domain representations of a second derivative Gaussian monocycle with centre frequency of 3.9 GHz.

This time is adjusted to permit a portion of the multipath components to pass before the transmission of the next pulse. Defining R as the data rate, and N_s the number of transmissions per symbol, the frame duration T_f and chip duration T_c can be written as

$$T_f = \frac{1}{N_s R}, \qquad (3)$$

$$T_c = \frac{1}{N_h N_s R}. \qquad (4)$$

For the purpose of this paper, the pulse shape was set as the second derivative of the Gaussian pulse, with centre frequency f_0, defined as [24]

$$w(t) = \left[1 - 2(\pi t f_0)^2\right] \exp\left\{-(\pi t f_0)^2\right\}, \qquad (5)$$

with energy normalised Fourier transform of

$$\widetilde{W}(f) = \sqrt{\sqrt{\frac{32\pi f_o^2}{3}} \frac{2}{\sqrt{\pi f_o^2}} \left(\frac{f}{f_0}\right)^2 \exp\left\{-\frac{f^2}{f_0^2}\right\}}. \qquad (6)$$

Figure 2 presents the time domain representation of the energy normalised Gaussian waveform, with its corresponding power spectral density. A monocycle width of 0.5 nanosecond was selected, corresponding to a centre frequency of approximately 3.9 GHz.

Applying the standardised IEEE 802.15.3a UWB channel model, the discrete impulse response of the propagation medium can be expressed as

$$h(u; x, t) = \sum_{l=0}^{L-1} \alpha_l(u; x) \delta(t - \tau_l), \qquad (7)$$

where x is the position of the receiver, and L is the number of paths in the discrete version of the response. Path delay τ_l is defined as $\tau_l = \tau \cdot l$, where τ represents the time separation between multipath components. Coefficients $\alpha_l(u; x)$ encompass the channel energy, defined as

$$E_{H, u; x} = \sum_{l=0}^{L-1} \left| \alpha_l(u; x) \right|^2. \qquad (8)$$

The received signal within a UWB system for N_u simultaneous users is defined as

$$
\begin{aligned}
r(t) &= \sum_{u=1}^{N_u} \sqrt{E_{\text{TX}}(u)} \sum_{m=0}^{N-1} w\left(t - mT_f - c_m^{(u)} T_c - \varepsilon b_m^{(u)}\right) \\
&\quad \otimes h(u; x, t) + n(t) \\
&= \sum_{u=1}^{N_u} \sqrt{E_{\text{TX}}(u)} \sum_{m=0}^{N-1} \sum_{l=0}^{L-1} \alpha_l(u; x) w\left(t - mT_f - c_m^{(u)} T_c \right. \\
&\quad \left. - \varepsilon b_m^{(u)} - \tau_l\right) + n(t),
\end{aligned}
\qquad (9)
$$

where $\otimes$ represents convolution, and the channel is assumed static over the transmission of each block of N frames. A RAKE receiver combines the dispersed energy among N_B of the L received paths, thus requiring N_B correlator branches, each aligned in time with their respective multipath component. An All-RAKE receiver considers all replicas of the transmitted signal ($N_B = L$); a Selective-RAKE receiver accounts for $N_B < L$ paths, considering the N_B paths with largest magnitude $\alpha_l(u; x)$; and finally a Partial-RAKE receiver combines energy from the first N_B paths only ($0 \le l < N_B$).

This paper focuses on the performance of an All-RAKE receiver.

2.3. Transmitter-side equalisation

Within a TR-UWB scheme, the time reversed complex conjugate of the forward link channel response is used to diversify the signal before transmission. In order to draw a correspondence with an All-RAKE receiver structure, all L multipath components were incorporated into the transmit prefilter. An alternate prefilter design is presented in [25], based upon a digital FIR filter.

The discrete representation of the time-reversed channel is defined as

$$h(u; x, -t) = \sqrt{E_{H, u; x}} \sum_{l=0}^{L-1} \beta_l(u; x) \delta(t - \tau_l), \qquad (10)$$

where

$$\beta_l = \alpha_{(L-1)-l}. \qquad (11)$$

The channel response is assumed known at the transmitter side. Estimation of the response can be achieved through the use of the theory of reciprocity for antennas and electromagnetic propagation. It states that the outputs of nonlinear antennas for identical excitation signals, as detected at the other

antenna, will be identical provided the medium between the antennas is linear and isotropic [26]. Conversely, more accurate channel knowledge can be obtained through receiver-side feedback to the transmitter.

The signal transmitted per user is given by

$$
\begin{aligned}
s_{\text{TR}}^{(u)}(t) &= \sqrt{\frac{E_{\text{TX}}(u)}{E_{H,u;x}}} \left(\sum_{m=-\infty}^{\infty} w\big(t - mT_f - c_m^{(u)}T_c - \varepsilon b_m^{(u)}\big) \right) \\
&\quad \otimes h^*(u;x,-t) \\
&= \sqrt{\frac{E_{\text{TX}}(u)}{E_{H,u;x}}} \sum_{m=-\infty}^{\infty} \sum_{l=0}^{L-1} \beta_l(u;x) w\big(t - mT_f - c_m^{(u)}T_c \\
&\qquad\qquad\qquad\qquad - \varepsilon b_m^{(u)} - \tau_l\big),
\end{aligned}
\tag{12}
$$

where the division with $E_{H,u;x}$ is needed to normalise the energy of the channel response. This is to ensure that the energy transmitted remains equal to $E_{\text{TX}}(u)$.

Without loss of generality, user 1 is taken as the desired user, with the signal detected at its receiver in location x_1 given by

$$
\begin{aligned}
r_{\text{TR}}(t) &= \left(\sum_{u=1}^{N_u} s_{\text{TR}}^{(u)}(t) \otimes h(u;x_1,t) \right) + n(t) \\
&= \left(\sum_{u=1}^{N_u} \sqrt{\frac{E_{\text{TX}}(u)}{E_{H,u;x_1}}} \sum_{m=-\infty}^{\infty} R_{h(1)h(u)}\big(t - mT_f - c_m^{(u)}T_c - \varepsilon b_m^{(u)}\big) \right. \\
&\qquad\qquad\qquad\qquad\qquad \left. \otimes w(t) \right) + n(t),
\end{aligned}
\tag{13}
$$

where

$$
R_{h(1)h(u)}(t) = h(1;x_1,t) \otimes h^*(u;x_1,-t)
\tag{14}
$$

is the correlation of the channel impulse responses from the 1st and the uth user to user 1's receiver at location x_1. It should be noted that all transmitters were assumed dispersed enough such that the channel responses from each N_u transmitter to any receiver are independent. Additive white Gaussian noise with variance of $N_0/2$ is also present.

The decision variable (Z) is constructed through the multiplication of the received signal with the receiver template, giving the estimated received data of $\hat{b}_m^{(u)}$

$$
\begin{aligned}
Z_{\text{TR}}^{(u)} &= \int_{(m-1)T_f + c_m^{(u)}T_c + \tau_{(L-1)}}^{(m-1)T_f + c_m^{(u)}T_c + \tau_{(L-1)} + 2T_m} \\
&\quad \times r_{\text{TR}}(t) g\big\{ t - \big[(m-1)T_f + c_m^{(u)}T_c + \tau_{(L-1)}\big] \big\} dt,
\end{aligned}
\tag{15}
$$

where

$$
\hat{b}_m^{(u)} = \begin{cases} 0, & Z \geq 0, \\ 1, & Z < 0, \end{cases}
\tag{16}
$$

$$
g(t) = w(t) - w(t - \varepsilon).
\tag{17}
$$

It can be seen in (15) that there is an additional shift of τ_{L-1} for the integration, which is required to align the template with the largest peak in the received signal of the desired user. The $(L-1)$th path is the in-phase autocorrelation peak position for the channel response, referred to as the main lobe. The template $g(t)$ was adapted for free-space propagation in order to draw an equivalence between an All-RAKE dependent UWB system, and the time-reversed method. When the guard time T_g is chosen such that ISI is avoided, an All-RAKE-UWB and a TR-UWB system exhibit identical diversity orders and thus have the same error performance, even in the presence of multiuser interference (MUI). However, temporal focusing allows TR-UWB to be more resilient in the presence of ISI, as will be shown through simulation in Section 4.

With the received signal taking the form of the autocorrelation of the channel impulse response, it can be inferred that inherent sidelobe energy will exist. Following from this, it can be seen that increasing the randomness of a channel response results in lower sidelobe energy. Thus, an NLOS system is expected to out-perform an LOS system. However, larger lengths of the NLOS channels will ultimately lead to an increase in the duration of the sidelobe energy.

While not studied in this paper, a TR-UWB system may adopt only a portion of the channel response as the signal prefilter. An analysis into time-reversed systems utilising only selected paths of the channel, also referred to as "dynamic TR," can be found in [6, 15].

For a further comparison between transmitter- and receiver-side equalisation, consider the system models for UWB and TR-UWB in Figures 3(a)–3(d). It can be noted that the main variations are the added prefiltering in the TR-UWB transmitter, and subsequently simplified receiver structure relative to the N_B branch RAKE receiver in Figure 3(b). For brevity, frame- and time-hopping shifts have been omitted in the receiver structures.

Hereafter, a chip synchronous single-input-single-output (SISO) system is considered, assuming that the transmit and receive antennas, which would act as pulse shaping filters, have no significant combined effect on the signal transmitted. Time-reversal properties also apply in an SISO system, assuming that the bandwidth occupied by transmissions is much larger than the correlation frequency exhibited by the channel [27]. Also, a quasistationary channel is assumed, such that it remains time-invariant for the transmission of a full UWB packet. Calculations are based upon the CM1 channel scenario of the 802.15.3a model, characterised for an LOS system with a 0–4 m separation between all transmit and receive pairs.

3. ERROR PERFORMANCE ANALYSIS

3.1. Time-hopping code analysis

With all users assumed to be transmitting the same level of energy, and influenced by the same channel model, the remaining influential factor on the level of intersymbol and
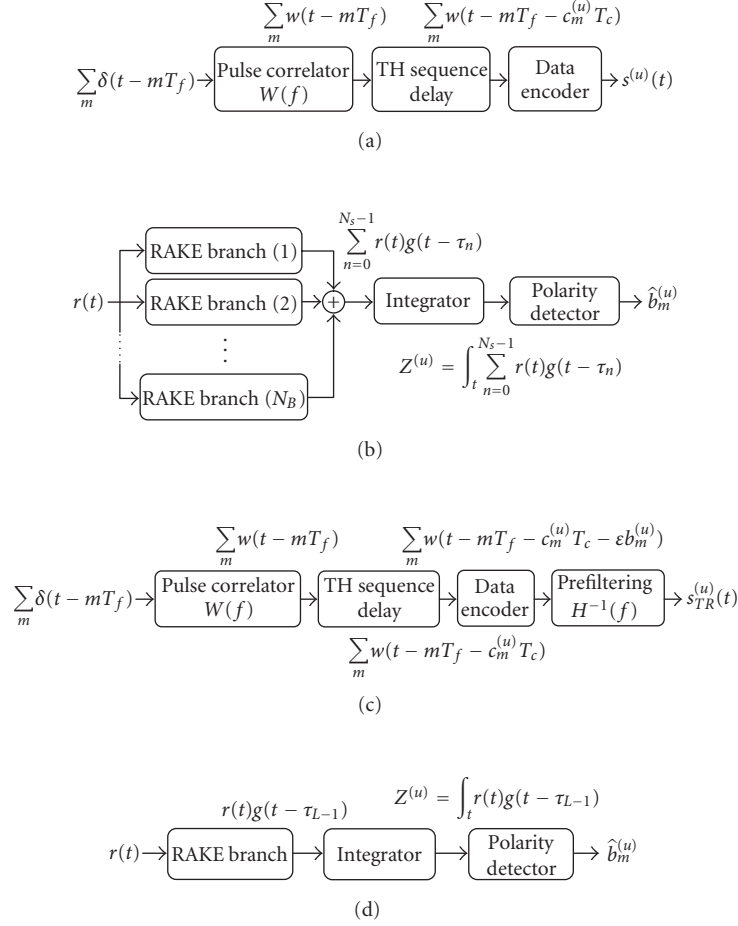
$$\sum_m w(t - mT_f) \qquad \sum_m w(t - mT_f - c_m^{(u)} T_c)$$

$\sum_m \delta(t - mT_f) \rightarrow$ [Pulse correlator $W(f)$] $\rightarrow$ [TH sequence delay] $\rightarrow$ [Data encoder] $\rightarrow s^{(u)}(t)$

(a)

[RAKE branch (1)]
$r(t) \rightarrow$ [RAKE branch (2)] $\rightarrow (+) \rightarrow$ [Integrator] $\rightarrow$ [Polarity detector] $\rightarrow \hat{b}_m^{(u)}$
[RAKE branch (N_B)]

$$\sum_{n=0}^{N_s-1} r(t)g(t - \tau_n)$$

$$Z^{(u)} = \int_t \sum_{n=0}^{N_s-1} r(t)g(t - \tau_n)$$

(b)

$$\sum_m w(t - mT_f) \qquad \sum_m w(t - mT_f - c_m^{(u)} T_c - \varepsilon b_m^{(u)})$$

$\sum_m \delta(t - mT_f) \rightarrow$ [Pulse correlator $W(f)$] $\rightarrow$ [TH sequence delay] $\rightarrow$ [Data encoder] $\rightarrow$ [Prefiltering $H^{-1}(f)$] $\rightarrow s_{TR}^{(u)}(t)$

$$\sum_m w(t - mT_f - c_m^{(u)} T_c)$$

(c)

$$r(t)g(t - \tau_{L-1}) \qquad Z^{(u)} = \int_t r(t)g(t - \tau_{L-1})$$

$r(t) \rightarrow$ [RAKE branch] $\rightarrow$ [Integrator] $\rightarrow$ [Polarity detector] $\rightarrow \hat{b}_m^{(u)}$

(d)

FIGURE 3: System model for (a) UWB transmitter, (b) UWB receiver, (c) TR-UWB transmitter, and (d) TR-UWB receiver.

multiuser interference is the time-hopping code. The cardinality of the hopping code is generally chosen to be equal to the number of chips within a single frame (N_s). In order to predict the performance of a perfectly power controlled system, the hopping code itself must be analysed.

Intersymbol and multiuser interferences are affected by the separation between consecutive elements within sequences. These indicate the number of intermediary chips between transmissions by a single user for ISI and chip separations between different users for MUI. Figure 4 illustrates the ISI separation for two transmissions, separated by A frames.

The chip separation probability ($S_e(A, B)$) is determined for a certain separation B between transmissions, where A represents the number of intermediate frames. The issue of intermediate pulses over the separation distance is important since the RMS delay spread of a signal may cause intersymbol interference well over an adjacent frame. These probabilities are determined through a brute force analysis of the hopping code ($c_m^{(u)}$) used for multiuser encoding, averaged over the all codes within each family of sequences. Evaluated state probabilities for the given A are $[p_1, p_2, \ldots, p_{2(N_h-1)+1}]$, where $S_e(A, B) = p_B$. For ISI, each code within a sequence
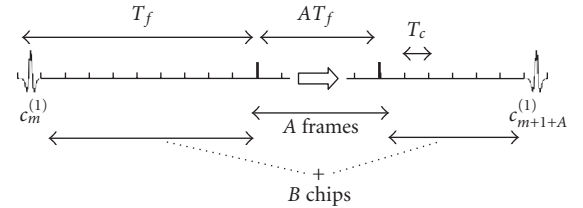

FIGURE 4: Symbol separations.

family is analysed separately, while for MUI all possible sequence pairs are considered.

Probabilities are significantly dependent upon the cardinality (N_h) of the hopping code. A larger value will result in more chips to select from, leading to a more sparse profile. The separation between any two user transmissions ranges from AN_h to $(A + 2)N_h - 2$, where A is zero for adjoining frames.

This paper focuses on Reed-Solomon [28] and linear congruence [29] hopping codes. A discussion on the relative performance of various sequences in a time-hopped environment can be found in [30]. The ISI chip separation
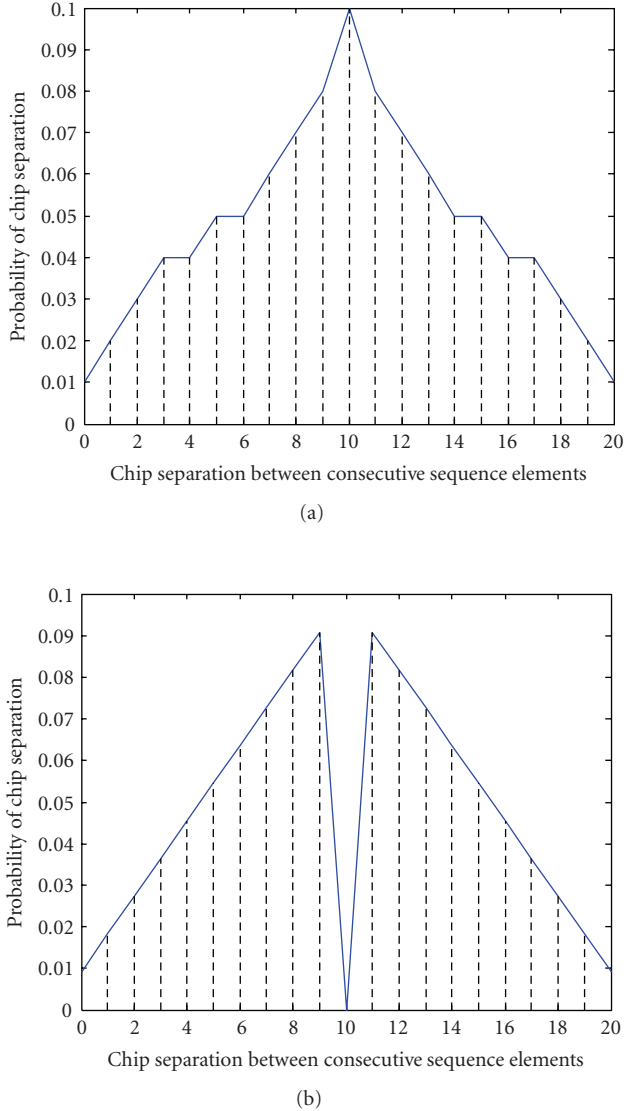
(a)

(b)

Figure 5: Chip separation probabilities for (a) Reed-Solomon and (b) linear congruence codes.

probabilities for these sequence families for a cardinality of $N_h = 11$, no intermediary pulses ($A = 0$), and separation ranging from 0 to $2N_h - 2$ are given in Figures 5(a) and 5(b), respectively.

3.2. Intersymbol interference

Considering typical RMS delay spread for a UWB multipath channel, intersymbol interference may cause a significant degradation. This is particularly evident in TR-UWB systems, with a larger transmitted waveform close to doubling the length of the received signal. ISI is affected by the width of the transmitted pulses, and the data rate. The level of interference will diminish to zero provided that the chip time is greater than twice the length of the channel response

($2L\tau$), allowing enough time for the multipath components to pass.

In order to estimate the performance of a TR-UWB system operating in a scattering environment, the expected ISI variance may be determined. This is accomplished by estimating the level of interference for a single transmission, summed over all overlapping adjacent transmissions by the same user. In order to obtain a close approximation, the ISI must be Gaussian distributed.

The ISI estimation in this paper takes an average on the ε shift introduced for the encoding of data. Assuming independent identically distributed random variables for $b_m^{(u)}$, this average is equivalent to no data modulation shift.

With the received signal comprised of Gaussian waveforms, which ideally have a zero average, the ISI has an expected mean of zero. This reduces the variance calculation to

$$\sigma^2 \equiv \langle (Y - \mu)^2 \rangle = \langle Y^2 \rangle, \tag{18}$$

where μ represents the signal mean, and $\langle \cdot \rangle$ an ensemble average. The variance is calculated over all overlapping transmissions, also over all possible chip separations by applying the probabilities determined in Section 3.1.

The formula for the variance of the ISI, averaged over N transmissions, is given by (19), which accounts for interference from preceding transmissions (Pre ISI) and following transmissions (Post ISI). Parameters N_w and N_l define the number of paths expected to overlap for the pre- and post-transmission ISI, respectively, with N_{ov} representing the number of adjacent frames over which the transmitted signal will exist. It should be noted that the transmission channel and the prefiltering channel are identical for ISI;

$$\sigma_{ISI}^2 = \sum_{\sigma=1}^{N_{ov}} \sum_{\varsigma=1}^{(2(N_h-1)+1)} (\chi_{\sigma,\zeta,\xi} + \chi_{\sigma,\zeta,\psi}), \tag{19}$$

where

$$\chi_{\sigma,\zeta,\nu} = S_e(\sigma - 1, \varsigma) \cdot \text{var}\left(h(1; x_1, t) \otimes \left[\sqrt{\frac{E_{TX}(1)}{E_{H,1;x_1}}} \cdot \nu \right] \right),$$

$$\xi = \sum_{k=N_w}^{L-1} \beta_{k+1} w(t - \tau_{k-N_w}),$$

$$\psi = \sum_{k=0}^{N_l-1} \beta_{k+1} w(t - \tau_{k+N_w}),$$

$$N_w = \left\lceil \frac{(\sigma - 1)T_f + \varsigma T_c}{\tau} \right\rceil,$$

$$N_l = L - N_w,$$

$$N_{ov} = \left\lceil \frac{L\tau}{T_f} \right\rceil.$$

Here, ν represents the portion of the transmitted signal which is regarded as ISI, and is referred to as the third parameter of $\chi_{\sigma,\zeta,\nu}$. This formula converges to an ISI variance within 5% of the final value when averaged over approximately 50 iterations.

3.3. Multiuser interference

Within an environment where multiple users operate in close proximity, there is the possibility of interuser interference. For the case of ISI, if the chip time T_c is greater than the transmission duration $L\tau$, interference is of no concern. For MUI, this condition would only remove the partial interference caused by transmissions in adjacent chips, while the issue of same chip collisions between users remains. For a multiuser scenario, there are three types of interference which must be accounted for: in-phase, where two users transmit in the same chip; pre-out-of-phase, interference caused by signals in previous chips; and post-out-of-phase, interference caused by signals in subsequent chips.

The first is dependent upon the separation probabilities of user asynchronisation within a single frame; while the latter two are dependent upon possible separations between users for frames over which a transmission exists. Since user asynchronisation is assumed uniform, the separation probability vector $S_e(A,B)$ will be identical for in-phase and out-of-phase interference.

The MUI variance estimation presented here accounts for the interference by a single user only, with the result scaled. The in-phase variance given by (20) encompasses interference from transmissions within the same frame as the desired user. Only the partial overlap is considered for each possible separation Θ, determined as in the ISI case by the parameters $N_{w(\text{In})}$, which represents the number of paths before an overlap of the preinterference occurs; and $N_{l(\text{In})}$, which indicates the number of paths which are overlapping for post-interference. The out-of-phase MUI expression in (21) accounts for overlapping from frames adjacent to the desired user's transmission. For each MUI type, the expected interference signal is convoluted with the channel response from the interferer to the desired user's receiver at position x_1, and the energy normalised;

$$\sigma^2_{\text{InPhaseMUI}} = \sum_{\Theta=-(N_h-1)}^{0} \chi_{\Theta,\xi} + \sum_{\Theta=1}^{N_h-1} \chi_{\Theta,\psi}, \qquad (20)$$

where

$$\chi_{\Theta,\nu} = S_e\big(0, \Theta+(N_h-1)+1\big) \cdot \mathrm{var}\Big(h(u;x_1,t) \otimes \Big[\sqrt{\tfrac{E_{\text{TX}}(u)}{E_{H,u;x_1}}} \cdot \nu\Big]\Big),$$

$$\xi = \sum_{k=N_{w(\text{In})}}^{L-1} \beta_{k+1} w\big(t - \tau_{k-N_{w(\text{In})}}\big),$$

$$\psi = \sum_{k=0}^{N_{l(\text{In})}-1} \beta_{k+1} w\big(t - \tau_{k+N_{w(\text{In})}}\big).$$

For the out-of-phase counterpart

$$\sigma^2_{\text{OutPhaseMUI}} = \sum_{\sigma=1}^{N_{\text{ov}}} \sum_{\varsigma=1}^{(2(N_h-1)+1)} \big(\chi_{\sigma,\zeta,\xi} + \chi_{\sigma,\zeta,\psi}\big), \qquad (21)$$

where

$$\chi_{\sigma,\zeta,\nu} = S_e(0,\varsigma) \cdot \mathrm{var}\Big(h(u;x_1,t) \otimes \Big[\sqrt{\tfrac{E_{\text{TX}}(u)}{E_{H,u;x_1}}} \cdot \nu\Big]\Big),$$

$$\xi = \sum_{k=N_{w(\text{Out})}}^{L-1} \beta_{k+1} w\big(t - \tau_{k-N_{w(\text{Out})}}\big),$$

$$\psi = \sum_{k=0}^{N_{l(\text{Out})}-1} \beta_{k+1} w\big(t - \tau_{k+N_{w(\text{Out})}}\big),$$

with

$$N_{w(\text{In})} = \Big\lceil -\Theta \cdot \tfrac{T_c}{\tau} \Big\rceil,$$

$$N_{l(\text{In})} = L - N_{w(\text{In})},$$

$$N_{w(\text{Out})} = \Big\lceil \tfrac{(\sigma-1)T_f + \varsigma T_c}{\tau} \Big\rceil,$$

$$N_{l(\text{Out})} = L - N_{w(\text{Out})},$$

$$N_{\text{ov}} = \Big\lceil \tfrac{L\tau}{T_f} \Big\rceil.$$

Thus the final variance formula equates to the expected interference from a single interferer, multiplied by the number of interferers, evaluated as

$$\sigma^2_{\text{MUI}} = \big(\sigma^2_{\text{InPhaseMUI}} + \sigma^2_{\text{OutPhaseMUI}}\big) \cdot (N_u - 1). \qquad (22)$$

Through testing, it was determined that an MUI variance within 5% of the final value could be obtained after approximately 100 iterations.

The N_l, N_w, and N_{ov} path alignment parameter variations for both ISI and MUI formulation are illustrated in Figure 6, with a time-reversed transmission approximated by a triangular waveform. Three consecutive chip aligned transmissions are shown for a single user, together with randomly shifted transmissions from one interfering user ($u \neq 1$). The dark shading represents the desired signal, while the light shading indicates the interference sources from both ISI and MUI.

3.4. Error analysis

For a binary PPM UWB system sending N_s transmissions per symbol, the probability of error is determined through [31]

$$P_e = Q\big(\sqrt{N_s \cdot \text{SINR}}\big) = \tfrac{1}{2}\mathrm{erfc}\Big(\sqrt{\tfrac{N_s \cdot \text{SINR}}{2}}\Big), \qquad (23)$$
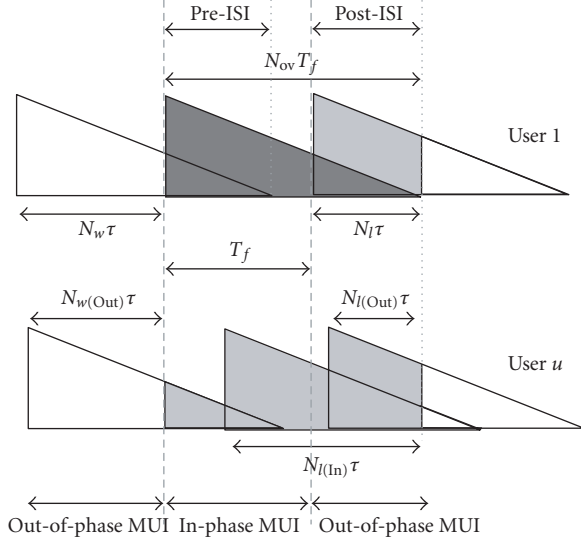
FIGURE 6: Path alignment parameters for ISI and MUI variance formulation.

FIGURE 7: Similarity analysis of UWB and TR-UWB in the absence of ISI at 3 Mbit/s, $N_s = 1$.

where SINR represents the signal-to-combined noise, ISI, and MUI ratio. Note that this is for "soft" signal reception, where the signal formed by N_s pulses is observed as a single multi-pulse transmission. This is in contrast to "hard" signal detection, where independent decisions are computed over each of the N_s transmissions, and then a majority criterion applied to determine the encoded data [32].

In order for (23) to hold, it must be true that all parameters of the SINR are Gaussian distributed. The additive white noise exhibited by the system is defined as a statistically independent zero mean Gaussian random variable. The ISI and MUI terms may be brought under the standard Gaussian approximation provided that the number of paths within the channel impulse responses, the number of transmissions per symbol, the number of interfering users, and bit rate for all transmitters are sufficiently large [33]. For all testing purposes, the number of paths within the channel responses was set at 40, and a maximum of 10 users were tested. Since the noise and interference terms are assumed Gaussian, and the signal transmitted is deterministic, the received signal is also Gaussian distributed.

Although the received signal power $P_{RX}(u)$ may arrive at the receiver, only the power in the main autocorrelation peak is used for data decoding $((L-1)$th path). This is accounted for by an additional ratio "ϕ," determined by observing the ratio of main path to sidelobe power over several tests. For the LOS, 0–4 m channel scenario of the IEEE 802.15.3a model, $\phi \approx 0.566$, averaged over 50 independent realisations of the model. The final SINR is

$$\text{SINR} = \frac{\phi \cdot P_{RX}(u)}{\sigma_{ISI}^2 + \sigma_{MUI}^2 + \sigma_{AWGN}^2}, \tag{24}$$

with $\sigma_{MUI}^2 = 0$ for a single user system.

4. COMPARISON OF SIMULATED AND ESTIMATED RESULTS
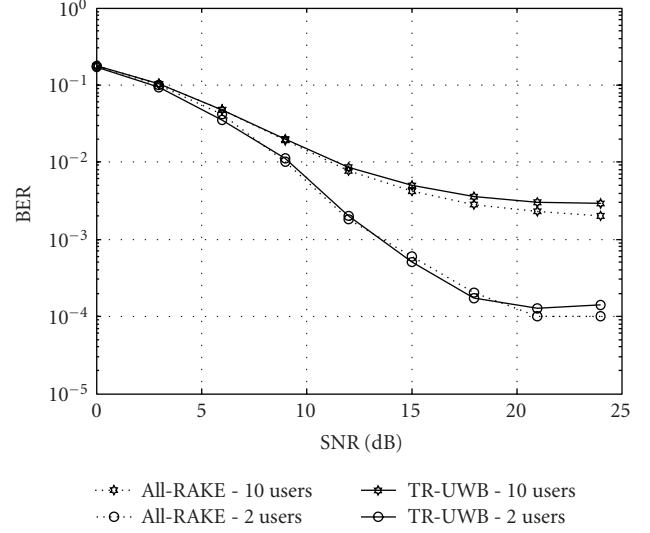
All-RAKE and TR-UWB simulations were adapted from a time hopped PPM UWB simulation by Di Benedetto and Giancola [32]. The cardinality and periodicity of each time hopping code were set to 11, with a pulse width T_m of 0.5 nanosecond, and a data encoding shift ε of 0.5 nanosecond. The multipath time separation parameter τ was set to 1 nanosecond, chosen to be greater than the base waveform width, and to allow an encoded signal to be orthogonal to its nonencoded counterpart. All users had equal transmit powers of 1 mW, and equal data rates which were adjusted by changing the frame width T_f. The packet size was set constant at 1024 octets.

In order to ensure the equivalence of the UWB and TR-UWB models in the absence of ISI, simulations were conducted at a data rate of 3 Mbit/s, $N_s = 1$, for 2 and 10 users, with results shown in Figure 7. This data rate and N_s combination allows the majority of the 40 nanoseconds channel response tested to pass before the transmission of the next symbol. Equality between the two methods is shown in the presence of varied MUI, where the use of time hopping allows the system to exhibit a comparatively reasonable performance for a 10-user scenario.

The ISI variance equation was tested by observing the performance of a simulated single user scenario. Resulting error rates using Reed-Solomon time hopping for the All-RAKE and TR-UWB simulations, together with the TR-UWB variance equation ("TR-Equ"), are shown in Figures 8 and 9 for an N_s of 5 and 10, respectively. It can be observed that for all tested data rates, the semianalytical analysis closely traces the simulated performance. Also, equivalent All-RAKE based systems exhibit severely impaired performance in the presence of increased ISI. This difference
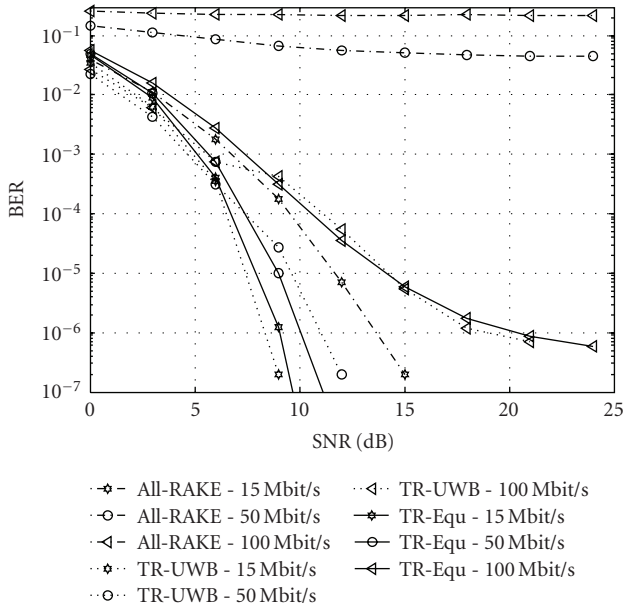
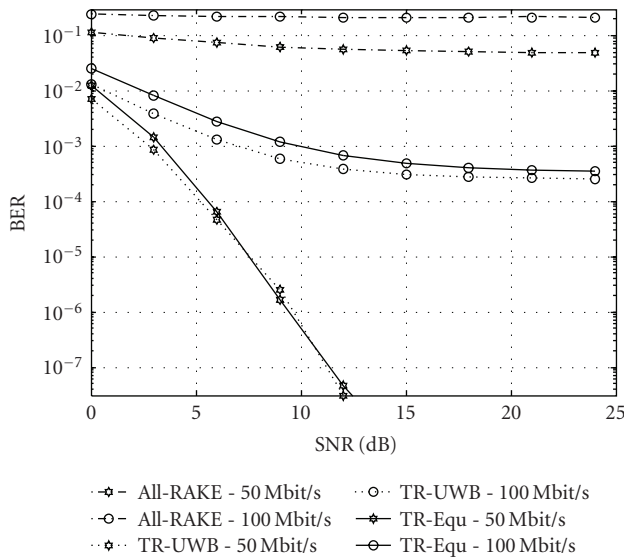FIGURE 8: BER curves for ISI with Reed-Solomon coding ($N_s = 5$).

FIGURE 10: BER curves for ISI and MUI for Reed-Solomon coding at 30 Mbit/s, $N_s = 5$.

FIGURE 9: BER curves for ISI with Reed-Solomon coding ($N_s = 10$).
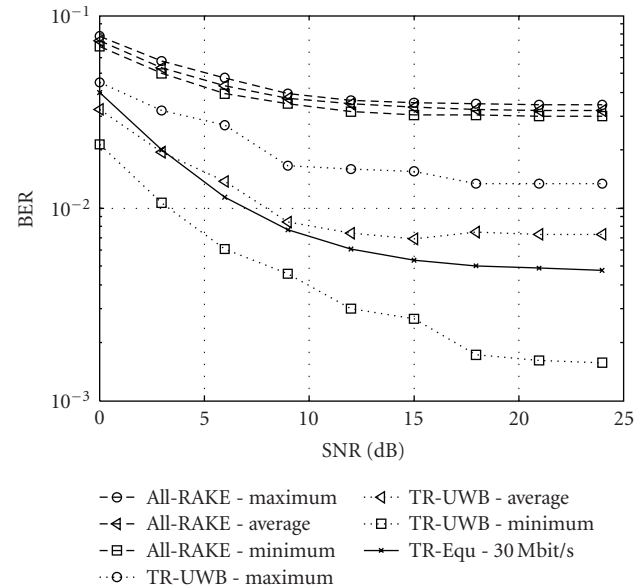
FIGURE 11: BER curves for ISI and MUI for Reed-Solomon coding at 30 Mbit/s, $N_s = 10$.

intensifies for higher data rates, which leads to a proportional elevation in the level of ISI. These results are supported by RAKE and TR-UWB tests in the presence of ISI conducted in [25].

Through (3), it was seen that the parameter N_s also affects the frame length. At a data rate of 100 Mbit/s, the ISI plateau is clearly visible. For $N_s = 5$, the formulated plateau occurs at approximately 10^{-6}, while for $N_s = 10$ it appears at nearly 10^{-4}.
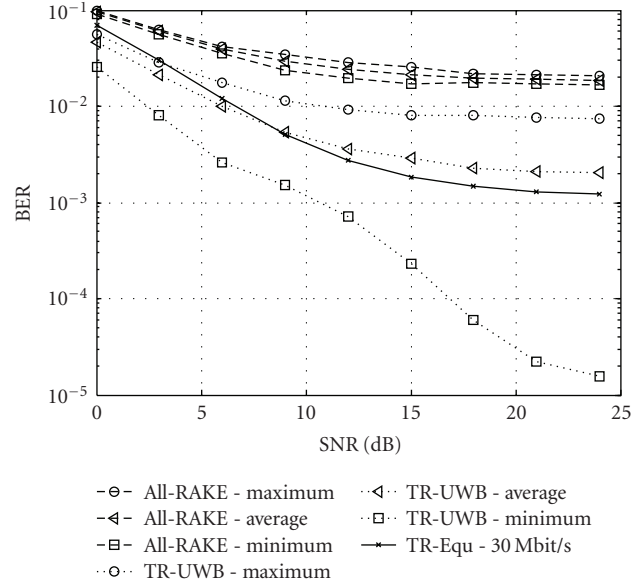
MUI variance tests were conducted at a data rate of 30 Mbit/s, with $N_s = 5$ and 10. Results are illustrated in Figures 10 and 11. The plots indicate the maximum, minimum, and average BER rates over all users for both All-RAKE and TR-UWB simulations, and also the average performance as based on the TR-UWB variance formulas. It is evident that the formulated curve closely follows the average simulated performance. At 30 Mbit/s, $N_s = 10$, it can be seen that the derived curve follows the median of the maximum and
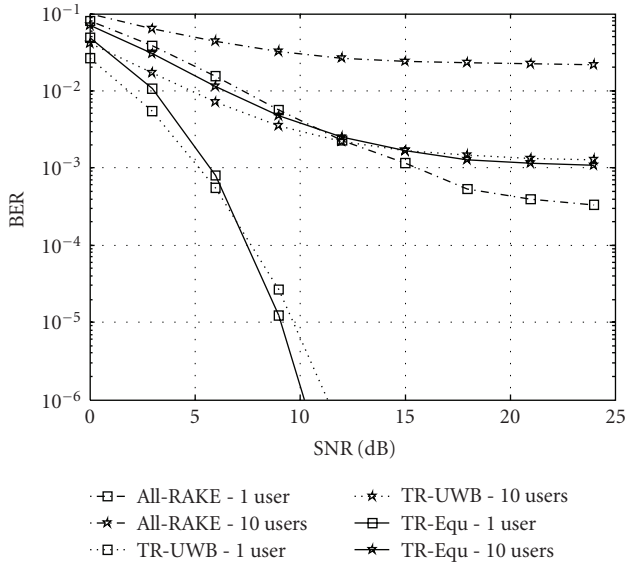
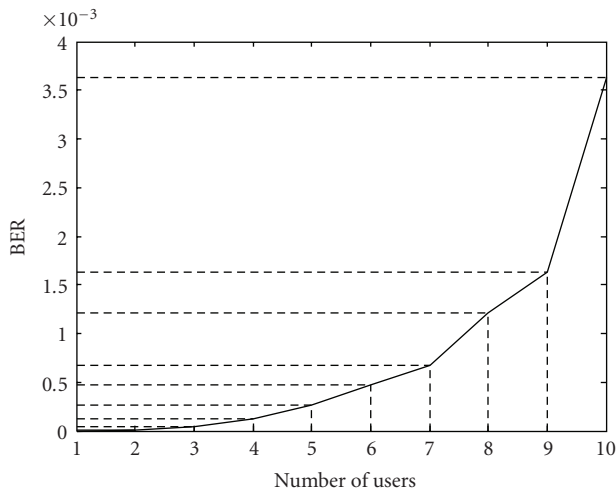FIGURE 12: BER curves for 1-user and 10-user cases with linear congruence coding at 30 Mbit/s, $N_s = 5$.

FIGURE 13: BER versus number of users at 12 dB, 30 Mbit/s, $N_s = 5$.

In order to examine the performance of this system with varied hopping schemes, "linear congruence" hopping codes were also tested. Results for 1 and 10 user tests, at a data rate of 30 Mbit/s and $N_s = 5$, are shown in Figure 12. The equivalence between the formulated and simulated results can be seen. While the maximum and minimum error rates for the 10-user case are not shown, an alignment with the average BER is apparent. The prevailing difference in performance between All-RAKE and TR-UWB is once again evident.

Figure 13 indicates the effects of MUI on the expected performance of a time reversed system at 30 Mbit/s, $N_s = 5$, with a signal-to-noise ratio of 12 dB. The addition of each user results in an increase in the level of MUI present, following a near exponential rise in the error rate. Although a time-reversed system does have the benefit of mitigating ISI, further measures are required to reduce the degrading effects of interfering users.

5. CONCLUSIONS

While a TR-UWB system does require increased processing at the transmitter side, it removes much of the burden from the receiver, and allows more robust operation in the presence of ISI. While this may only be a shift of requirement in a single-transmitter single-receiver system, it has significant benefits in single-transmitter multiple-receiver circumstances, such as cluster-based wireless actuator networks.

Through simulation, it was determined that derived equations for the variance of ISI and MUI closely follow expected results. Variance formulae take into consideration separation between user transmissions, together with chip separation probabilities, for both signal degradations. The capabilities of TR-UWB in mitigating ISI to a certain degree were shown, although exhibiting larger variance between user error performances in a multiuser case when compared to a system using an All-RAKE receiver.

Future work that can be conducted in this area includes independent transmitter-based time filtration to decrease the effect of multiuser interference on system performance. Also, a study into the validity of the Gaussian approximation assumed for varied system parameters, and the possibility of time-hopping code design based upon chip separation probability analysis, can be envisaged.

REFERENCES

[1] FCC News, "New Public Safety Applications and Broadband Internet Access among uses Envisioned by FCC Authorization of Ultra-Wideband Technology," Unofficial Announcement of Commission action, February 2002.

[2] FCC Document 00-163, "Revision of Part 15 of the Commission's Rules Regarding Ultra-Wideband Transmission Systems," April 2002, ET Docket No. 98-153.

[3] S. Lemon, "Standards deadlock hits UWB—the market will have to decide," IDG News Service, May 2005 http://www .techworld.com/applications/news/index.cfm?NewsID=3674.

[4] S. Deffree, "No standard for ultra wideband comms," January 2006, Electronic News, http://ElectronicsWeekly.com/.

minimum error rates. Due to MUI being dominant relative to ISI in the scenarios tested, there is a closer correspondence between All-RAKE and TR-UWB error rates than in a single user system, with errors due to ISI effects only.

Figures 10 and 11 also illustrate an interesting property about the variance between user performance in transmitter and receiver side equalisation types. While achieving relatively better performance, TR-UWB exhibits severe variations in the error probabilities between users. On the contrary, All-RAKE based UWB has a much fairer error distribution, although all users having relatively worse performance than a time reversed system.

[5] G. F. Edelmann, T. Akal, W. S. Hodgkiss, S. Kim, W. A. Kuperman, and H. C. Song, "An initial demonstration of underwater acoustic communication using time reversal," *IEEE Journal of Oceanic Engineering*, vol. 27, no. 3, pp. 602–609, 2002.

[6] K. Usuda, H. Zhang, and M. Nakagawa, "Pre-Rake performance for pulse based UWB system in a standardized UWB short-range channel," in *Proceedings of IEEE Wireless Communications and Networking Conference (WCNC '04)*, vol. 2, pp. 920–925, Atlanta, Ga, USA, March 2004.

[7] S. M. Emami, J. Hansen, A. D. Kim, et al., "Predicted Time Reversal Performance in Wireless Communications Using Channel Measurements," IEEE COMLET, 2002, http://www.nari.ee.ethz.ch/commth/pubs/files/TRComLet.pdf.

[8] R. C. Qiu, H. Liu, and X. Shen, "Ultra-wideband for multiple access communications," *IEEE Communications Magazine*, vol. 43, no. 2, pp. 80–87, 2005.

[9] T. Strohmer, M. Emami, J. Hansen, G. Papanicolaou, and A. J. Paulraj, "Application of time-reversal with MMSE equalizer to UWB communications," in *Proceedings of IEEE Global Telecommunications Conference (GLOBECOM '04)*, vol. 5, pp. 3123–3127, Dallas, Tex, USA, November-December 2004.

[10] M. Fink, "Time-reversed acoustics," *Scientific American*, vol. 281, pp. 91–97, 1999.

[11] G. Yue, L. Ge, and S. Li, "Performance of UWB time-hopping spread-spectrum impulse radio in multipath environments," in *Proceedings of the 57th IEEE Semiannual Vehicular Technology Conference (VTC '03)*, vol. 3, pp. 1644–1648, Jeju, Korea, April 2003.

[12] J. Foerster, "Channel modelling sub-committee report final," Report IEEE 802.15.SG3a, IEEE, New York, NY, USA, December 2002.

[13] M. Chen and X. Li, "Transmitter-based channel equalization and MUI suppression for UWB systems," in *Proceedings of the International Conference on Modern Problems of Radio Engineering, Telecommunications and Computer Science (TCSET '04)*, pp. 501–504, Lviv-Slavsko, Ukraine, February 2004.

[14] A. E. Akogun, R. C. Qiu, and N. Guo, "Demonstrating time reversal in ultra-wideband communications using time domain measurements," in *Proceedings of the 51st International Instrumentation Symposium*, pp. 737–742, Knoxville, Tenn, USA, May 2005.

[15] A. Derode, A. Tourin, and M. Fink, "Random multiple scattering of ultrasound. II. Is time reversal a self-averaging process?" *Physical Review E*, vol. 64, no. 3, Article ID 036606, 13 pages, 2001.

[16] S. Zhao and H. Liu, "Prerake diversity combining for pulsed UWB systems considering realistic channels with pulse overlapping and narrow-band interference," in *Proceedings of IEEE Global Telecommunications Conference (GLOBECOM '05)*, vol. 6, pp. 3784–3788, St. Louis, Mo, USA, November-December 2005.

[17] M. Z. Win and Z. A. Kostic, "Virtual path analysis of selective Rake receiver in dense multipath channels," *IEEE Communications Letters*, vol. 3, no. 11, pp. 308–310, 1999.

[18] ETH Zurich, "BTnodes—A Distributed Environment for Prototyping Ad Hoc Networks," 2005, http://www.btnode.ethz.ch/.

[19] Intel Corporation, "Intel Mote 2 Overview," 2005, http://www.intel.com/research/downloads/imote_overview.pdf.

[20] M. Z. Win and R. A. Scholtz, "On the energy capture of ultrawide bandwidth signals in dense multipath environments," *IEEE Communications Letters*, vol. 2, no. 9, pp. 245–247, 1998.

[21] T. Strohmer, M. Emami, J. Hansen, G. Papanicolaou, and A. J. Paulraj, "Application of time-reversal with MMSE equalizer to UWB communications," in *Proceedings of IEEE Global Telecommunications Conference (GLOBECOM '04)*, vol. 5, pp. 3123–3127, Dallas, Tex, USA, November-December 2004.

[22] A. G. Klein and C. R. Johnson Jr., "MMSE decision feedback equalization of pulse position modulated signals," in *Proceedings of IEEE International Conference on Communications (ICC '04)*, vol. 5, pp. 2648–2652, Paris, France, June 2004.

[23] T. Erseghe, "Time-hopping patterns derived from permutation sequences for ultra-wide-band impulse-radio applications," in *Proceedings of the 6th WSEAS International Conference on Communications*, vol. 1, no. 1, pp. 109–115, Crete, Greece, July 2002.

[24] A. Swami, B. Sadler, and J. Turner, "On the coexistence of ultra-wideband and narrowband radio systems," in *Proceedings of IEEE Military Communications Conference on Communications for Network-Centric Operations: Creating the Information Force (MILCOM '01)*, vol. 1, pp. 16–19, McLean, Va, USA, October 2001.

[25] N. Guo, R. C. Qiu, and B. M. Sadler, "An ultra-wideband autocorrelation demodulation scheme with low-complexity time reversal enhancement," in *Proceedings of IEEE Military Communications Conference (MILCOM '05)*, vol. 5, pp. 3066–3072, Atlantic City, NJ, USA, October 2005.

[26] C. A. Balanis, *Antenna Theory: Analysis and Design*, John Wiley & Sons, New York, NY, USA, 2nd edition, 1997.

[27] A. Derode, A. Tourin, J. de Rosny, M. Tanter, S. Yon, and M. Fink, "Taking advantage of multiple scattering to communicate with time-reversal antennas," *Physical Review Letters*, vol. 90, no. 1, Article ID 014301, 4 pages, 2003.

[28] R. M. Mersereau and T. S. Seay, "Multiple access frequency hopping patterns with low ambiguity," *IEEE Transactions on Aerospace and Electronic Systems*, vol. 17, no. 4, pp. 571–578, 1981.

[29] A. V. Jovancevic and E. L. Titlebaum, "New coding schemes for increased number of users or messages in frequency-hopped multilevel FSK," in *Proceedings of the 46th IEEE Vehicular Technology Conference (VTC '96), 'Mobile Technology for the Human Race'*, vol. 3, pp. 1732–1735, Atlanta, Ga, USA, April-May 1996.

[30] K. Popovski, B. J. Wysocki, and T. A. Wysocki, "Performance comparison of UWB hopping codes in a multi-user rich scattering environment," in *Proceedings of the 63rd IEEE Vehicular Technology Conference (VTC '06)*, vol. 4, pp. 1864–1868, Melbourne, Australia, May 2006.

[31] J. G. Proakis and M. Salehi, *Communication Systems Engineering*, chapter 7, Prentice-Hall, Englewood Cliffs, NJ, USA, 2nd edition, 2002.

[32] M-.G. Di Benedetto and G. Giancola, *Understanding Ultra Wide Band Radio Fundamentals*, Prentice-Hall Professional Technical Reference, Englewood Cliffs, NJ, USA, 2004.

[33] M.-G. Di Benedetto, "MAC for UWB," Networking with UWB - UWB Group at University of Rome, http://www.icsl.ucla.edu/~spapl/seminar/uwb2.pdf.